Proceedings of the
International Conference on Mechanical Engineering 2003
(ICME2003) 26- 28 December 2003, Dhaka, Bangladesh

ICME03-KEY-01

FLOW CHARACTERISTICS RELATED TO ARTERIAL DISEASES

Niranjan K. Talukder

Clark Atlanta University, Atlanta, Georgia 30314, USA

ABSTRACT

Arterial diseases may be related to flow characteristics induced by the local geometry of the flow channel. Initial stages of arteriosclerosis are found most frequently near branching sites and bends. A surgical anastomosis (cross-connecting vessel) may become partially or completely occluded due to thrombosis. The level of flow disturbance due to arterial constriction depends on the severity of constriction. Model experiments using flow visualization and hot-film techniques were performed that revealed secondary flow, flow separation and oscillating wall shear which may be involved in the initiation of arterial disease processes. Flow disturbance due to arterial stenosis (constriction) was performed applying Doppler ultrasound and digital signal processing. Preliminary results demonstrated a distinct increase in magnitude of a disturbance index as relative disturbance (RD) with increasing percentage area reduction or degree of stenosis (DOS). Efforts are underway to establish correlations between DOS and RD, which could be used in noninvasive diagnosis of DOS.

Keywords: Arterial diseases, Flow characteristics, Model experiments.

1. INTRODUCTION

Pathologic changes of arterial walls, manifest by high concentration of lipids, wall tissue hardening and thickening that may lead to partial occlusion are called arteriosclerosis. Atheroma or early stages of the disease occur most frequently near branching sites and bends, as illustrated in Figure 1. The predilection of atheroma for

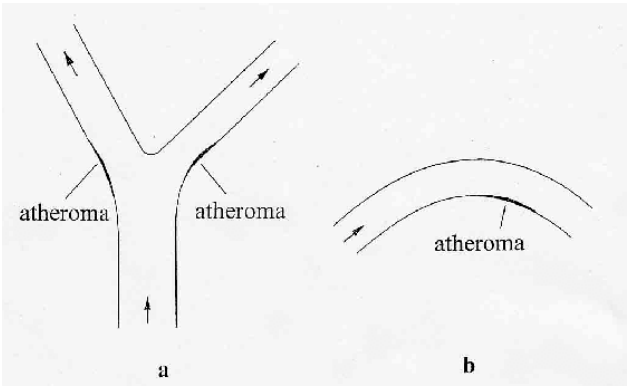

Figure 1. Predilection sites of atheroma
a) at a bifurcation and b) at a bend

certain locations in the vascular system was suspected to be related to flow phenomena induced by the local flow channel geometry. Although the biochemical processes that lead to the advance stages of the disease are very complex, the physical effects due to special flow phenomena on the mass transfer at the arterial wall was thought to play an important role in the initiation of the disease process. Some of the early model investigations on flow phenomena in a coronary artery bend and a branching site by Müller-Mohnssen [1] showed that the predilection sites of atheroma are regions of relatively low flow velocities. Fox and Hugh [2], performing flow visualization in two-dimensional bifurcation models, demonstrated that the predilection sites are coincident with flow separation zones with flow stasis, in favor of the view that deposition of particulate blood constituents causing thrombus formation might initiate atherogenesis. The deposition hypothesis was later further supported by flow visualization studies by Müller-Mohnssen [3] which indicate transport of blood constituents to the arterial wall by reattaching flow. Arteriosclerotic lesions were found to contain relatively high levels of cholesterol and phospholipids. While cholesterol appeared to be derived from the blood flow [4], accumulation of phosholipids in the lesions was found to be due to synthesis in the arterial wall [5]. It was thought that any direct or indirect effect of flow phenomena on mass transfer between blood and arterial wall may cause disturbance to normal wall tissue metabolism and thus be related to the disease. There was a consensus regarding the importance of the controlling role of the endothelial cell monolayer at the internal surface of the blood vessels in the mass transfer between blood and arterial wall. After Fry [6], performing *in vivo* experiments, demonstrated that elevated wall shear stress could cause deterioration of the endothelial surface, high shear was considered to be a possible initiator of arteriosclerosis. Caro et al. [7], on the other hand, showed *in vitro* that the wall shear at the predilection sites of atheroma is relatively low. These

investigators also proposed a shear dependent mass transfer for atherogenesis. Model studies of flow phenomena at arterial bifurcations by Talukder [8, 9] revealed secondary flow, flow separation and strong pulsation of wall shear stress at the predilection sites of atheroma. Talukder et al. [10] performed quantitative flow visualization in a carotid bifurcation model, tracking individual particles in the flow fields studied. Some particles were found to undergo very slow backward motion near the carotid sinus wall and to have relatively long residence time in the carotid sinus, in support of the deposition hypothesis.

Surgical bypass grafts or anastomoses may become partially or even completely occluded due to thrombosis. The flow phenomena at these artificial branchings were considered to have a significant influence on the thrombus formation and thus on the long-term patency of the grafts. The flow characteristics in vein grafts were investigated both *in vivo* and *in vitro* models [11, 12] for the different angles of anastomosis illustrated in Figure 2, in order to determine the effects of the angle of diversion on the flow field in the graft.

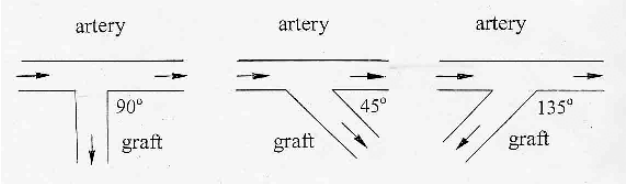

Figure 2. Schematics of grafts with different angles of diversion of the flow direction: a) 90°, b) 45° and c) 135° (arrows indicate flow directions)

The flow immediately downstream of vascular stenosis (constriction) is likely to be disturbed due to vortex shedding and eddy formation in the fluid layers between main stream and the surrounding separation zone, as illustrated in Figure 3.

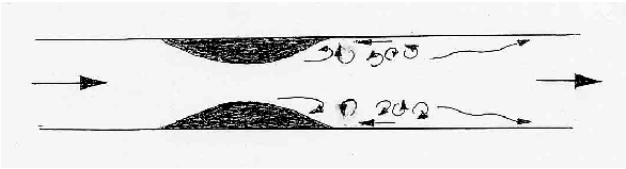

Figure 3. Schematic of flow disturbance due to vessel constriction

Talukder et al. [13] found that the flow fields distal to mild (<60% area reduction) arterial stenoses are characterized by certain phasic coherent structures, and that there is a distinct increase in random disturbance with increasing degree of stenosis (DOS) beyond 60% area reduction. Talukder and Talukder [14] defined a disturbance index as relative disturbance (RD) based on flow disturbance due to vessel constriction and, performing *in vitro* model studies, demonstrated a distinct increase in the value of RD with increasing DOS.

The present paper reviews some of the above earlier studies and discusses ongoing effort to analyze flow disturbance due to arterial stenosis with a view to establishing correlations between DOS and RD.

2. MODEL STUDIES OF FLOW AT ARTERIAL BRANCHING

To gain insight into the flow phenomena that may be related to the predilection of atheroma for arterial branching sites, model studies using different flow visualization techniques have been carried out by many investigators. One of the important conditions for similarity of flow phenomena is the geometry of flow channel which is considered next.

2.1 Branching geometry

Although the branching geometry may vary throughout the vascular system, there is in general a remarkable dependence of the branch angles (angles between the stem and the branches) on the relative branch diameters [15]. The branch with the smaller diameter has a larger angle with the stem than the branch with the larger diameter. If the branches are of approximately equal diameter, their angles with the stem are also approximately equal. Also, the total cross sectional area of the two branches is larger than the cross sectional area of the stem. The arterial bifurcation models used by Talukder [8, 9] were designed using the following relations:

$$A_1 + A_2 = 1.2A_0 \qquad (1)$$

and

$$A_2/A_1 = \sin\theta_1/\sin\theta_2 \qquad (2)$$

where A_0 is the cross sectional area of the stem, A_1 and A_2 are the cross sectional areas of the branches making the angles θ_1 and θ_2 with the stem, respectively, as illustrated in Figure 4.

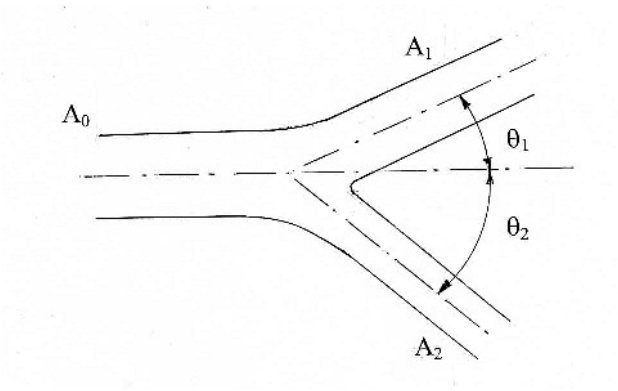

Figure 4. Branching angles and cross sectional areas

The above relations were based on anatomical data from a rabbit kidney [15]. While Eq. (1) represents an assumed average area increase, Eq. (2) satisfies lateral force balance at a bifurcation [8, 9]. For convenience of flow visualization, the stem diameter was chosen as 4

cm. The details of design and construction of the models were given in the appendix of [8].

2.2 Steady flow through symmetrical and asymmetric bifurcation

Beside geometric similarity of the models, the model flow conditions must correspond to the relevant range of mean Reynolds number Re given by

$$Re = v_m d/\nu \qquad (3)$$

where v_m is the mean velocity, d is the diameter of the vessel and ν is the kinematic viscosity of the fluid. The values of Re in most of the branched arteries in the human vascular system lie under 2000 and decrease towards the periphery due to decrease in both vessel diameter and mean flow velocity (increase in total area of cross section). For a 4-cm diameter model and water as model fluid, the mean flow velocity corresponding to a given Re is much smaller than in the arterial system. At Re =100, for example, the mean velocity in the stem of the model is about 2.5 mm/s.

Flow visualization was carried out using dilute fluorescent dyes (Fluorescin and Rhodamine B) which, due to very small density difference from water, are capable of following flow at velocities as low as 1 mm/s. Green fluorescent dye was introduced at a stem cross section several diameters upstream of the branching site using a dye introducing device with an array of eight capillary tubes arranged in a diametral plane which could be turned about the axis of the stem, in order to observe streaklines in various planes, including the plane of bifurcation. The dye holder was provided with a stopcock to start and end the dye introduction as desired. In addition to the array of green dye streaks, two orange fluorescent (Rhodamin B) dye streaks were introduced through capillaries arranged at some distance from the plane of bifurcation. Also, orange fluorescent dye could be introduced through several holes (1 mm diameter) at the outer wall of the branches, as desired.

The dye streaks were excited laterally, i.e., parallel to the plane of bifurcation using ultraviolet radiation and observed at right angle to the plane of bifurcation, whereby the glowing fluorescent dye streaks appeared bright on a darkened background.

In Figures 5 and 6 are illustrated some examples of flow patterns. Fig 5 shows flow patterns in a symmetrical model ($A_1=A_2$, $\theta_1=\theta_2=30^o$). Fig. 5a shows that the streaklines away from the plane of bifurcation have helical shapes. Fig. 5b shows that the streaklines in the plane of bifurcation get concentrated near the inner walls and rarefied near the outer walls. Also, there is flow separation from the outer wall in the left branch where the flow rate is lower (dye trapped in the separation bubble show rotation about a longitudinal axis and slow backward movement near the wall). Fig. 6 shows flow patterns in an asymmetric ($A_2=A_1/2$, $\theta_2=30^o$, $\theta_1=14.5^o$) model for unequal mean velocities in the branches. Note that there is flow separation from the outer wall of the branch of lower mean velocity (right branch in Fig. 6a, left branch ln Fig 6b, dye introduced through the outer wall as indicated by white arrows).

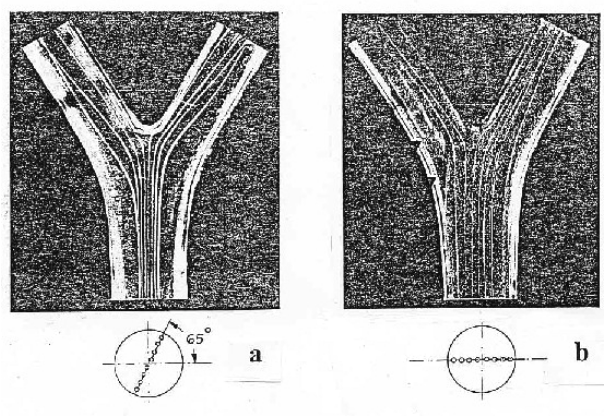

Figure 5 Flow patterns in a symmetrical ($A_2=A_1$) bifurcation model. a) $Q_2:Q_1=50:50$, b) $Q_2:Q_1=30:70$

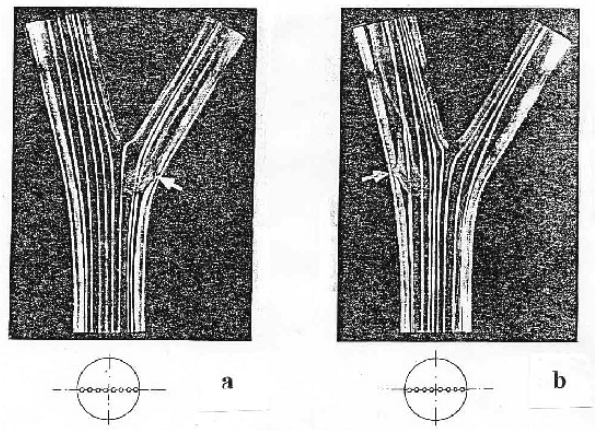

Figure 6 Flow patterns in an asymmetric ($A_2=A_1/2$) bifurcation model. a) $Q_2:Q_1=25:75$, b) $Q_2:Q_1=40:60$

From the above observations the following characteristics of branching flow can be recognized:

1. The streaklines in the plane of bifurcation remain in that plane but they get concentrated near the inner walls of the branches (near the flow divider) and rarefied near the outer walls, indicating high shear rates at the inner and low shear rates at the outer walls, as found by Caro et al. [7].
2. The streaklines away from the plane of bifurcation get helical shapes, indicating the presence of secondary flow, as expected in a bend (an arterial branching may be regarded as a set of two opposite bends fused together).
3. In the branch of lower mean velocity, the flow separates from the outer wall giving rise to a separation zone with back flow near the wall and rotation of the trapped fluid about longitudinal axes (spiral motion).

Velocity profiles in the plane of bifurcation were determined by recording the movement of the leading edges of eight streak lines simultaneously on a 16-mm

movie film and then analyzing the film frame-by-frame [8, 9]. They confirmed relatively high shear at the inner walls and low shear at the outer walls of the branches.

Although the above results obtained for steady flow supported the view that low shear might be the cause of predilection of atheroma for branching sites, that these were found to be sites of separated flow or recirculation zones, implied possible roles of reattachment, back flow near the wall and secondary flow in the mass transfer between blood and wall. Wall uptake was considered to be an important controlling factor in the transport process. Caro and Nerem [16] found that cholesterol uptake by an isolated dog common carotid artery perfused *in vitro* with serum containing labeled cholesterol was not diffusion controlled and suggested that an uptake-controlled transport could be shear dependent.

Also, the effects of flow pulsation on the fluid mechanical factors mentioned above and the reaction of the arterial wall to the local physical and chemical environment needed to be investigated before any clear conclusions could be drawn about their roles in atherogenesis.

2.3 Pulsatile flow through a symmetrical bifurcation

A flexible PVC model with 4 cm stem internal diameter and 3 cm branch internal diameter was used in this study [8]. Beside geometric similarity and mean Reynolds number, similarity of flow pulsation and the Womersley parameter (frequency parameter) α given by

$$\alpha = R[2\pi/(\nu T)]^{1/2}, \qquad (4)$$

where T is the period of pulsation, were taken into consideration. Physiologic flow pulsation was generated pneumatically and for flow visualization particles were suspended to the model fluid (75% glycerin-water mixture, $\nu = 0.2$ cm^2/s) with density match. The mean flow rate was adjusted to Re =400. A pulse period T=1 s, corresponding to α=11.2, was chosen.

The observations revealed oscillation of particles adjacent to the outer wall where separated flow and slow back flow had been observed for steady flow. These oscillations with two acceleration phases and two deceleration phases during a pulse period indicated high oscillatory wall shear with alternating direction from forward to backward twice each cycle.

Wall shear stresses were measured at one branch and at the stem using a DISA anemometer system consisting of a flush mounted hot-film probe (55 A 93), a temperature compensation probe, an anemometer bridge (55 D 01) and a linearizer (55 D 10) [8, 9]. The results confirmed oscillatory shear rates [8, 9]. Although the measurement yielded only the variable magnitude of wall shear and not its directions, from the flow visualization it was clear that the shear stress should not only have axial components (forward and backward) but also variable circumferential components due to secondary flow. In Fig. 7 is illustrated an example of the above [8, 9] wall shear stress variation over one period at a proximal point of the outer wall of one branch.

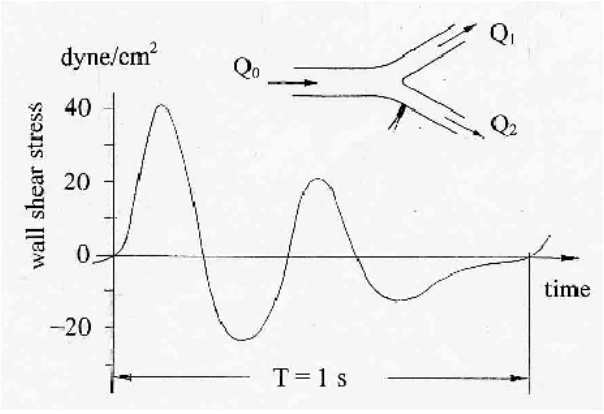

Figure 7. Pulsatile wall shear stress at the outer wall of a branch of the PVC model used. The probe location is indicated in the inset at the top, Q_2:Q_1=30:70

It was suggested [8, 9] that oscillation of wall shear stress at the sites of flow separation might affect mass transfer between blood and arterial wall at the separation zones and thus play an important role in the process of atherogenesis, although the mechanisms involved were not yet clear.

Measurement of pulsatile flow velocities in a carotid bifurcation model, applying laser Doppler anemomtry, by Ku and Giddens [17] confirmed the presence of oscillatory wall shear stress at the sites of atheroma predilection. Oscillatory wall shear with axial and circumferential components, implying continuously changing direction of wall shear stress, might affect shear-dependent wall uptake control that had been suggested by Caro and Nerem [16]. As found by Dewey, et al. [18], Nerem et al. [19], Davies et al. [20], Levesque and Nerem [21] and Helmlinger et al. [22], wall shear can affect endothelial cell morphology, orientation and function. Endothelial cells become elongated and aligned in the direction of wall shear. At the sites of continuous change in wall shear direction and magnitude, the endothelial cells may be in disorder and have altered cell function. Thus the special wall shear characteristics at the atheroma predilection sites may be linked to altered permeability or other uptake behavior of the endothelial barrier, leading to arterial diseases.

2.5 Particle paths in a carotid artery bifurcation

Beside shear-dependent wall permeability or uptake behavior, near-wall concentration and residence time of certain blood components was also thought to play possible roles in the disease process. One of the most commonly affected areas is the carotid sinus. Talukder et al. [10] explored the flow field in a glass model of the carotid bifurcation (31 mm common carotid diameter) by introducing individual, neutrally buoyant tracer particles (diameter 200 micron approx., specific gravity 1.05 approx.) into the flow (40% glycerin-water mixture, specific gravity 1.05 approx., ν =0.04 cm^2/s) at a common carotid cross section and tracking the particle paths in the carotid sinus. For α=5.0, the

corresponding model pulse period would be 15 s. However, in this study only steady flow phenomena at Re=400, 600 and 800 were investigated. The movements of individual particles, in side view and reflected top view, were recorded on a 16 mm film using a Bolex (H 16) movie camera. Particle paths and speeds were determined from frame-by-frame analysis of the recordings.

Depending on their individual particle positions at the entry cross section, the particles were found to move along various complicated paths with variable speeds and direction of motion. Some particles were found to undergo very slow backward motion near the sinus wall and have relatively long residence times in the sinus [10]. Figure 8 illustrates the projected locus (top view) of one such particle. The position of the particle in the common carotid is shown in a cross sectional view (section 0-0).

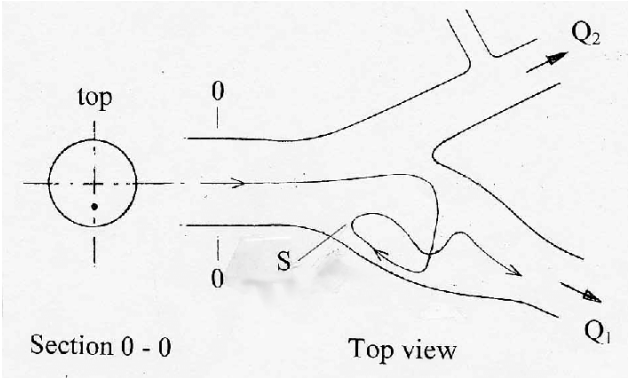

Figure 8. Projection of particle locus in a model carotid sinus. Position of the particle in the common carotid is shown in a sectional view (0-0). Q_1:Q_2=70:30, S shows approximate location of slowest motion

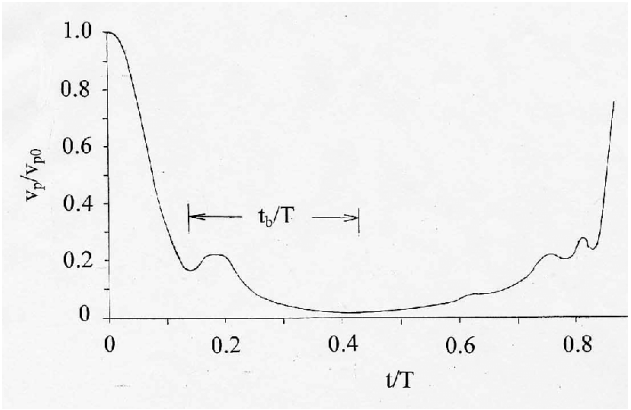

Figure 9. Normalized particle speed as a function of normalized time. Approximate normalized period of backward motion t_b/T is shown

Figure 9 shows the variation of the particle speed v_p along the locus in the sinus region normalized with the particle speed v_{p0} at the cross section 0-0 (Fig. 8). The time scale is normalized with the corresponding pulse period of pulsatile flow (T= 15 s). Note that there is a considerable period of slow backward motion, the lowest normalized speed of the particle being on the order of 2% and occurring at about the end of this period. The corresponding particle position is shown by S in Fig. 8 (near the point of turning from backward to forward motion)

The drastically reduced speed and relatively long residence time of blood components including platelets may conduce platelet aggregation and thrombus formation. Thrombosis may lead to partial or even complete vessel occlusion within relatively short times.

3. FLOW CHARACTERISTICS IN ARTERIAL ANASTOMOSES

Long-term patency of surgical anastomoses may largely depend on the thrombogenic properties of the grafts. However, certain flow characteristics such as large flow separation zones are considered to induce thrombosis and should be avoided. Flow fields in the grafts are likely to depend on the graft angle. An acute angle of diversion from the supplying artery was thought to have advantage over 90°, while obtuse angles were thought to be worse than 90°.

Talukder and Nerem [12] investigated the flow in vein graft models with the angles of anastomoses illustrated in Fig. 2. Since the frequency parameter is small ($\alpha < 3$) for the relevant arteries ($d < 0.5$ cm), only steady flow in the Reynolds number range of clinical interest ($100<Re<400$) was studied. A plexiglass model with 5.08 cm internal diameter (both artery and graft) was used in this study. Flow visualization was performed using fluorescent dyes, fluorescin (green) and Rhodamin B (orange), for different flow rate ratios between artery and graft. Velocity profiles in the plane of anastomosis were measured applying hot-film anemometry. The results revealed interesting flow characteristics some of which were unexpected, as described in the next subsection.

3.1 Flow patterns and velocity profiles in anastomoses

In Figure 10 are illustrated the flow patterns in graft models with different graft angles.

For 90° anastomosis (Fig. 7a), a large separation zone with slow back flow at the proximal wall of the graft was observed, as expected (the point of dye introduction at the proximal wall of the graft is recognized as a bright spot from where the dye is seen to move backward before tuning forward around a large separation bubble). For 45° angle of diversion (Fig. 7b), the separation zones were found to be unexpectedly large and spread over relatively large areas of the graft wall (note the back flow of dye near the wall from a point about 2.5 diameters from the corner), indicating no improvement of the flow field as to inducing thrombus formation. On the other hand, for 135° angle of diversion (Fig. 7c), the separation zones were found to be surprisingly small and covering remarkably small areas of the graft wall (note the forward flow of dye near the wall from a point only 1.5 diameters from the corner). The reason for the suppression of the separation bubble in the case of a large angle of turning

of the fluid from the artery to the graft is the presence of relatively strong secondary flow.

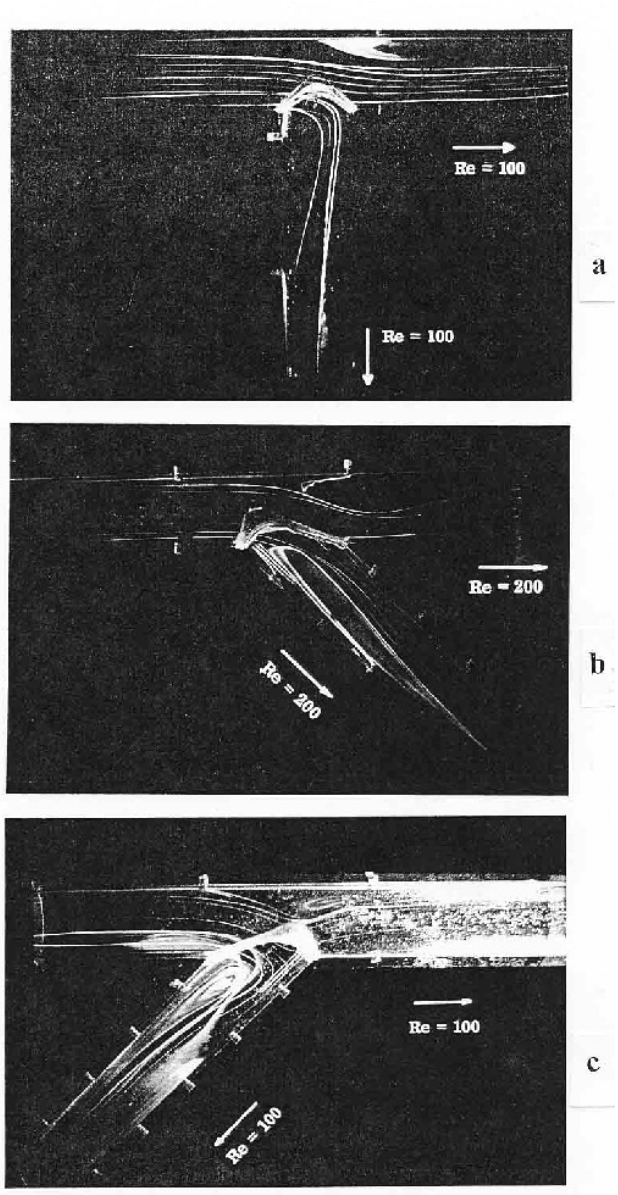

Figure 10 Flow patterns in graft models with a) 90°, b) 45° and c) 135° angle of diversion

The above phenomena, were confirmed by measured velocity profiles in the plane of anastomosis of each of the graft models used at a proximal cross section I as indicated in Fig. 11. Flow velocities were measured at discrete points (up to 19) across the diameter of each graft model using an L-shaped hot-film anemometer probe in conjunction with a DISA bridge (55D01) and a DISA linearizer (55D10). Some of the velocity profiles obtained were presented in reference [12]. Each of these profiles was found to be skew with the maximum velocity shifted towards the distal wall of the graft and revealing very low negative velocities closer to the proximal wall (indicated by P in Fig. 11) consistent with the flow visualization. While for 90° and 45° angles of flow diversion the zone of low backward velocity was relatively wide, for 135° there were very narrow zones of slow back flow, if at all. Figure 11 shows a comparison of some of the above [12] velocity distributions.

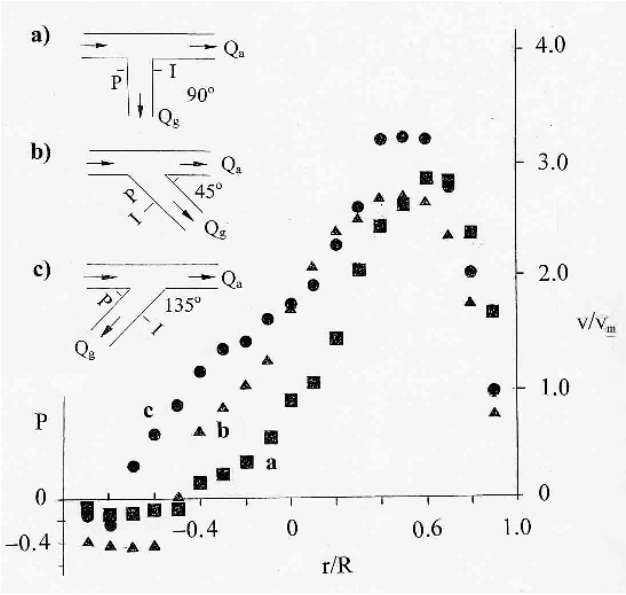

A

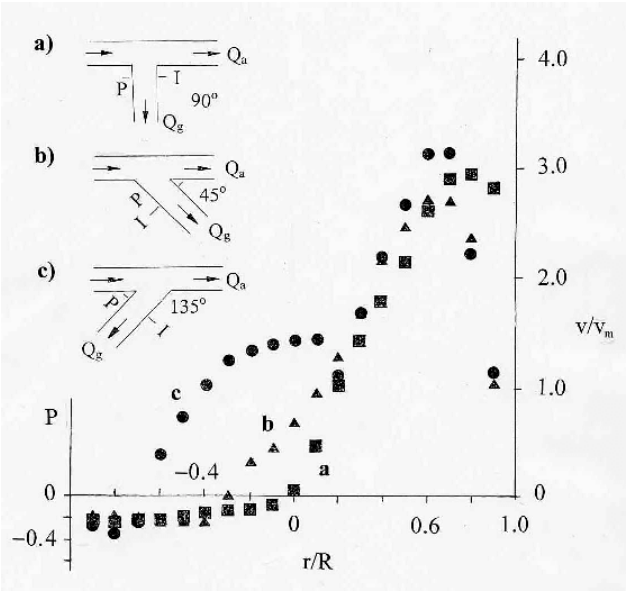

B

Figure 11. Comparison of measured velocity distributions across graft diameter at cross section I. Velocity v is normalized by the corresponding mean velocity v_m. A) $Re_g=Re_a=100$, B) $Re_g=Re_a=200$. P indicates proximal side

Based on the above results of flow visualization and velocity measurement, it appeared that a graft with a large (>90°) angle of turn of the flow direction should not be inferior and might even be preferable.

4. FLOW DISTURBANCE DUE TO ARTERIAL CONSTRICTION

Arterial constrictions are likely to cause flow disturbance, i.e., velocity fluctuation, due to vortex shedding and instability of the poststenotic diverging flow (see Fig. 3). A noninvasive measurement of blood flow velocity fluctuations just downstream of a constriction could lead to a noninvasive assessment of the severity of constriction. Ultrasound velocimeters are widely used in percutaneous measurement of blood flow in peripheral arteries and could be employed for velocity disturbance measurement as well.

Ultrasound velocimetry is based on the Doppler effect, i.e., the frequency shift between the emitted and reflected ultrasound, which is proportional to the velocity of reflecting particles suspended in the fluid. Referring to Figure 12, the relation between the frequency shift f (Doppler frequency) and the flow velocity v (velocity of the reflecting particles) may be given as

$$f = 2vf_o\cos\theta \ / \ c, \qquad (5)$$

where f_o is the frequency of the emitted ultrasound, θ is the angle between the ultrasound beam and the velocity of the reflecting particles and c is the sound speed in the fluid medium.

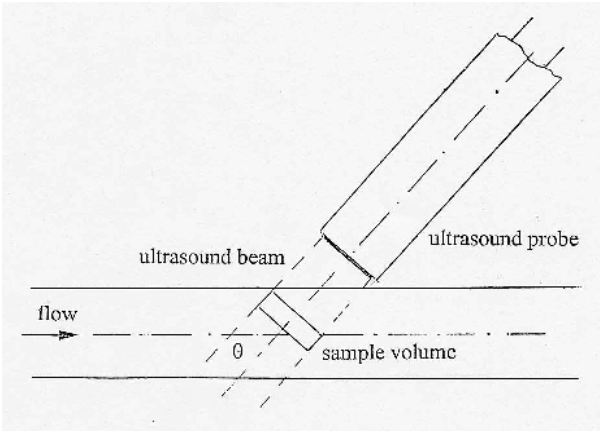

Figure 12. Ultrasound probe orientation to flow channel

The variation of the Doppler frequencies obtained from a given sample volume during a given sampling period depends on the variation of the velocities of the different reflecting particles within the sample volume during the sampling time. The mean frequency shift f_m, which is a measure of the mean velocity within the sample volume during the sampling period, may be obtained from the corresponding power spectrum P(f) using the relationship

$$f_m = \int f\,P(f)df \,/\, \int P(f)df \qquad (6)$$

whereby the limits of integration (not shown) are the minimum and maximum relevant frequencies with appreciable power within the power spectrum.

Usually continuous wave Doppler ultrasound systems are used to measure average velocity at a vessel cross section. Although an increased average velocity is an indicator of local vessel constriction this method is inadequate for accurate assessment of the degree of stenosis, i.e., the percent area reduction. A range gated pulsed Doppler ultrasound system, on the other hand, can provide information on flow velocities at discrete positions within a vessel cross section. Since high-frequency fluctuation of velocity at a certain location is an indication of flow disturbance, an analysis of flow disturbance based on the second moment of Doppler frequency power spectra was proposed by Talukder and Talukder [14]. The theoretical basis, and procedure used in that earlier study as well as ongoing effort to establish correlations between degree of stenosis and a relative disturbance are described in the following subsections.

4.1 Theoretical basis for analysis of flow velocity disturbance using Doppler frequency spectra

For a pulsatile flow, as in the arteries, spatial and temporal variation of velocity within a finite sample volume and during a finite sampling period is bound to cause a certain variation in the Doppler frequency obtained even when the flow is normal, i.e., the artery is not at all constricted. For an undisturbed flow, the deviations of the velocities from the mean velocity within a sample volume and during a sampling period are expected to be relatively small and hence the corresponding power spectra are expected to be relatively narrow. With increasing level of flow disturbance (deviations of velocities from the mean), there should be a broadening of Doppler frequency power spectrum. Since the level of flow disturbance is expected to rise with the severity of vessel constriction, i.e., degree of stenosis (DOS), spectral broadening (SB) is expected to increase with DOS. A quantitative SB may be given by [14]

$$SB = [\ \int (f - f_m)^2 P(f)df \,/\, \int P(f)df\ ]^{1/2}. \qquad (7)$$

The ratio of SB to f_m, which may be regarded as relative disturbance (RD), is obtained from Eqs. (7) and (6), after simplification, as

$$RD = (I_1 I_3 / I_2^2 - 1)^{1/2}, \qquad (8)$$

where

$$I_1 = \int P(f)df, \qquad (9)$$

$$I_2 = \int fP(f)df, \qquad (10)$$

and

$$I_3 = \int f^2 P(f)df. \qquad (11)$$

For any given power spectrum, first the above three integrals may be evaluated, and then RD can be calculated using Eq. (8). Note that RD is dimensionless and depends only on the relative power variation over frequencies and not on absolute magnitudes or unit of power in a power spectrum.

4.2 Model experiments

The experimental setup used in the ongoing study of flow disturbance just downstream of arterial stenosis models, a modification of the one used in earlier studies [13, 14], is illustrated in Figure 13. A silicon rubber tube of 0.635 cm internal diameter is used as arterial model. Axisymmetric as well as eccentric stenosis models with different area reduction have been made out of silicon rubber cylinders of 0.714 cm outer diameter and 1.27 cm length. The new models have gradual area change distributed over a length equal to two vessel diameters, in contrast to those in earlier studies [13, 14] in which a thread wrapped around the vessel was applied to produce stenosis. They can be conveniently inserted into the flow system as connecting tubes between two parts of the silicon rubber (artery model) and exchanged during a series of experiments. To represent 0% stenosis, a 1.27 cm long PVC tube with 0.635 cm internal diameter and 0.794 cm outer diameter is used as connecting tube. The vessel segment where the stenosis models are inserted as well as the ultrasound emitter is kept immersed under water in a water-filled tray. The flow system is driven by a roller pump. Flow pulsation is generated using an electronically controlled solenoid valve. The minimum flow rate and thus also the mean flow rate is adjusted with the help of a bypass control clamp.

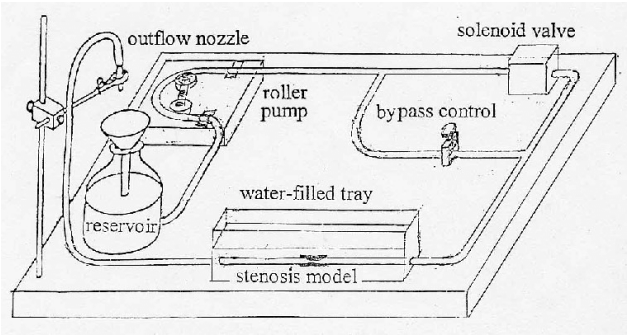

Figure 13. Schematic of experimental setup for studying flow disturbance due to arterial stenosis

The model fluid used is an aqueous solution of glycerin (40% glycerin) to which corn starch particles (1 teaspoon per liter) are added as ultrasound reflector. Flow rates are adjusted to satisfy Re <500 and a pulse period T=1 s was chosen to ensure α <3, corresponding to flow conditions in human peripheral arteries.

An 8-MHz range gated, pulsed Doppler ultrasound system with a pencil probe is used in the present study, as in an earlier study [14]. The probe alternately emits ultrasound at 8-MHz and receives reflected ultrasound which may have different frequencies due to Doppler shift caused by reflectors of different velocities. The electrical output signals of the system, which contain components having Doppler frequencies due to the motion of the particles suspended in the model fluid, are recorded on an analog magnetic tape and analyzed offline.

4.3. Signal processing and evaluation of RD

The first step in signal processing is the elimination of background noise, retaining the frequencies that are directly related to the velocity fluctuations studied (50 Hz – 10 kHz). The next step is to obtain power spectra of the signals. Efforts are being made to develop an integrated system for signal processing and evaluation of RD. In an earlier study [14] a PC audio card was used for analog-to-digital conversion of the signals and power spectra were obtained by performing FFT using Mathcad 3.1 software package. For each power spectrum obtained, RD was computed using Eqs. (8), (9), (10) & (11). Preliminary results [14] showing a distinct increase of RD with DOS, are presented in Table 1.

Table 1: Increasing value of RD with increasing DOS

DOS	20%	40%	60%	80%
RD	0.114	0.159	0.211	0.353

Investigations using the new stenosis models are underway, to verify the above trend and to establish correlations between DOS and RD.

5. ACKNOWLEDGMENT

This work was partially supported by the Boeing Company Support Program for Faculty Research.

6. REFERENCES

1. Müller-Mohnssen, H., 1958, "Die Strömungs-verhältnisse in den Coronararterien und ihre Bedeutung für die Manifestierung der Coronarsklerose", In: Lochner, W. and Witzleb, E. (eds.), *Probleme der Coronardurchblutung*, Springer Verlag, pp. 179-196.
2. Fox, J. A. and Hugh, A. E., 1966, "Localization of atheroma: A theory based on boundary layer separation", Brit. Heart J., 28:388-399.
   Müller-Mohnssen, H., 1976, "Experimental results to the deposition hypothesis of atherosclerosis", Thromb. Res., 8:553-566.
3. Newman, H. A. I. and Zilversmit, D. B., 1962, "Quantitative aspects of cholesterol flux in rabbit atheromatous lesions", J. Biol. Chem. 237:2078-2084.
4. Ziversmit, D. B., McCandless, E. L., Jordan, P. H., Henly, W. S. and Ackerman, R. F., 1961, "Synthesis of phospholipids in human atheromatous lesions", Circulation, 23:370-.375
5. Fry, D. L., February 1968, "Acute vascular endothelial changes associated with increased blood velocity gradients", Circ. Res., XXII:165-197.
6. Caro, C. G., Fitz-Gerald and Schroter, 1971, "Atheroma and arterial wall shear: Observation, correlation and proposal of a shear dependent mass transfer mechanism for atherogenesis", *Proc. Roy. Soc*. Lond. B. 177:109-159.
7. Talukder, N., 1974, "Untersuchung über die Strömung in arteriellen Verzweigungen",

Dissertation, Technical University of Aachen, Aachen, Germany.
8. Talukder, N., 1975, "An investigation on the flow characteristics in arterial branchings", ASME paper No. 75-APMB-4.
9. Talukder, N., Giddens, D. P. and Vito, R. P., 1983, "Quantitative flow visualization studies in a carotid artery bifurcation model", *Proc. Biomechanics Symposium*, AMD-Vol. 56/FED-Vol. 1, pp. 165-168.
10. Rittgers, S. E., Karayannacos, P. E., Talukder, N., Barrera, J. G. and Nerem, R. M., 1977, "In vivo and in vitro model studies of flow characteristics in arterial vein grafts", In: Grood, E. S. and Smith, R. C. (eds.), *Advances in Bioengineering*, ASME, pp. 27-29.
11. Talukder, N. and Nerem, R. M., 1978, "Flow characteristics in vascular graft models", *Digest of the 1st Int. Conf. Mechanics in Medicine and Biology*, Witzstrock Publ. House, pp. 281-284.
12. Talukder, N., Fulenwider, J. T., Mabon, R. F. and Giddens, D. P., August 1986, "Poststenotic flow disturbance in the dog aorta as measured with pulsed Doppler ultrasound", J. Biomech. Eng., Trans. ASME, 108:259-265.
13. Talukder, N. and Talukder, K., 1994, "Doppler frequency spectral broadening as an indicator of the severity of arterial stenoses", *Proc. 3rd Int. Symp. on Biofluid Mechanics*, Ser. 17, No. 107, VDI Verlag, pp.375-379.
14. Roux, W., 1895, "Gesammelte Abhandlungen über Entwicklungsmechanik der Organismen", Vol. 1, Publ. by W. Engleman Verlag.
15. Caro, C. G. and Nerem, R. M., 1973, "Transport of ^{14}C-4-cholesterol between serum and wall in perfused dog common carotid artery", Circ. Res., XXXII: 187-205.
16. Ku, D. N. and Giddens, D. P., 1987, "Laser Doppler anemometer measurements of pulsatile flow in a model carotid bifurcation", J. Biomechanics, Vol. 20, No. 4, pp. 407-421.
17. Dewey, Jr., C. F., Bussolari, S. R., Gimbrone, Jr., M. A. and Davis, P. F., August 1981,"The dynamic response of vascular endothelial cells to fluid shear stress", J. Biomech. Eng., Trans. ASME, 103:177-185.
18. Nerem, R. M., Levesque, M. J. and Cornhill, J. F., August 1981, "Vascular endothelial morphology as an indicator of the pattern of blood flow", J. Biomech. Eng., Trans. ASME, 103:172-176.
18. Davies, P.F., Dewey, Jr., C. F., Bussolari, S. R., Gordon, E. J. and Gimbrone, Jr., M. A., April 1984, "Influence of hemodynamic forces on vascular endothelial function-In vitro studies of shear stress and pinocytosis in bovine aortic cells", J. Clin. Invest., 73:1121-1129.
19. Levesque, M. J. and Nerem. R. M., 1985, "The elongation and orientation of cultured endothelial cells in response to shear stress", J. Biomech. Eng., Trans ASME, 176:341-347
20. Helmlinger, G., Geiger, R. V., Schreck, S. and Nerem, R. M., May 1991, "Effects of pulsatile flow on cultured vascular endothelial cell morphology", J. Biomech. Eng., Trans ASME, 113:123-131.

7. NOMENCLATURE

Symbol	Meaning	Unit
A_o, A_1, A_2	Area of vessel cross section	(cm^2)
c	Speed of sound	(m/s)
d	Vessel diameter	(cm)
f	Doppler frequency	(Hz)
f_m	Mean frequency	(Hz)
f_o	Ultrasound frequency	(MHz)
I_1	Integral-1	(1/s)
I_2	Integral-2	($1/s^2$)
I_3	Integral-3	($1/s^3$)
P(f)	Normalized power	
Q_0, Q_1, Q_2, Q_a, Q_g	Flow rate	(cm^3/s)
R	Vessel radius	(cm)
r	Radial coordinate	(cm)
Re, Re_a, Re_g	Reynolds number	
T	Pulse period	(s)
t	Time	(s)
t_b	Time of backward motion	(s)
v	Flow velocity	(cm/s)
v_m	Mean flow velocity	(cm/s)
v_p, v_{p0}	Particle velocity	(cm/s)
α	Womersley parameter	
ν	Kinematic viscosity	(m^2/s)
θ	Probe angle	(^{o})
θ_1, θ_2	Branch angle	(^{o})